**Shahid Chamran University of Ahvaz**

## Journal of
## Applied and Computational Mechanics

Research Paper

# Investigation of the Static Bending Response of FGM Sandwich Plates

Lazreg Hadji[1,2], Vagelis Plevris[3], George Papazafeiropoulos[4]

[1] University of Tiaret, Department of Civil Engineering, BP 78 Zaaroura, Tiaret,14000, Algeria, Email: lazreg.hadji@univ-tiaret.dz

[2] University of Tiaret, Laboratory of Geomatics and Sustainable Development, Tiaret, 14000, Algeria

[3] Department of Civil and Environmental Engineering, Qatar University, Doha, Qatar, Email: vplevris@qu.edu.qa

[4] School of Civil Engineering, National Technical University of Athens, Athens, Greece, Email: gpapazafeiropoulos@yahoo.gr

**Abstract.** In the present work, a displacement-based high-order shear deformation theory is introduced for the static response of functionally graded plates. The present theory is variationally consistent and strongly similar to the classical plate theory in many aspects. It does not require the shear correction factor, and gives rise to the transverse shear stress variation so that the transverse shear stresses vary parabolically across the thickness to satisfy free surface conditions for the shear stress. By dividing the transverse displacement into the bending and shear parts and making further assumptions, the number of unknowns and equations of motion of the present theory is reduced a and hence makes them simple to use. The material properties of the plate are assumed to be graded in the thickness direction according to a simple power-law distribution in terms of volume fractions of material constituents. The equilibrium equations of a functionally graded plate are given based on the higher order shear deformation theory. The numerical results presented in the paper are demonstrated by comparing the results with solutions derived from other higher-order models found in the literature and the present numerical results of Finite Element Analysis (FEA). In the numerical results, the effects of the grading materials, lay-up scheme and aspect ratio on the normal stress, shear stress and static deflections of the functionally graded sandwich plates are presented and discussed. It can be concluded that the proposed theory is accurate, elegant and simple in solving the problem of the bending behavior of functionally graded plates.

**Keywords:** Sandwich Plates, Functionally Graded Materials, Higher-Order Plate Theory, Stress, FEA.

## 1. Introduction

Functionally graded materials (FGM) are a type of composites whose properties vary gradually though directions. These types of advanced materials have more strength than classical composites and do not have interface problems, in contrast with layered composites. Because of these advantages, the functionally graded materials have been subject of investigation for a few decades.

Sandwich plates are made up of two face sheets or skins that are bonded together with a core in between them. The face sheets transmit in-plane and shear loads, while the core separates the face sheets to withstand transverse normal and shear loads. The resulting structure exhibits a high bending stiffness with low specific weight [1], and thus find applications in fields such as aerospace and aeronautics, nuclear energy, military, and medicine, among others. A metal-ceramic-based functionally graded material has numerous industrial applications because when combined, metals provide high toughness while ceramics have high-temperature resistance [2]. Because of the different thermo-mechanical properties of metal and ceramics, an abrupt change in the metal and ceramics combination causes high-stress concentration at the face sheet and core interface, which leads to delamination [3]. Hence, it is preferred to select either the skins or the core to be made of functionally graded materials.

Some researchers have investigated the bending of the FG plates by employing the plate theories. The most fundamental deformation theory is classical plate theory (CPT) which assumes that the plane normal to the mid plane before bending remains plane and normal after bending. This approach neglects the effect of all transverse stresses and it is therefore less accurate. Hence, it yields accurate results for the case of thin plates only. Javaheri and Islami [4] have obtained the static response of FGPs using CPT. The disadvantage of CPT was overcome by the first-order shear deformation theory (FSDPT) proposed by Reissner [5] and Mindlin [6] which considers the effect of transverse shear deformation. This theory does not satisfy the stress-free boundary conditions on the surfaces of the plate and requires an arbitrary shear correction factor. To avoid the use of shear correction factors, several higher-order shear deformation plate theories (HSDTs) have been proposed, such as the third order shear deformation theory (TSDPT) by Reddy [7], Tran et al. [8], Taj et al. [9], and Oktem et al. [10]. Various higher order shear deformation theories have been developed using five unknown functions. The theory presented by Houari et al. [11] is a new refined plate theory for bending response, buckling and free vibration of simply supported FGM sandwich plate with only four unknown functions. This theory is variationally consistent, does not require a shear correction factor, and gives rise to transverse shear stress variation such that the transverse shear stresses vary parabolically across the thickness, satisfying the shear stress-free surface conditions.

In recent years, many researchers have focused on studying the behavior of functionally gradient material structures; Shaat et al. [12] analysis size-dependent of functionally graded ultra-thin films. Malikan et al. [13] investigated a new hyperbolic-polynomial higher-order elasticity theory for mechanics of thick FGM beams with imperfection in the material composition. Golmakani et al. [14] developed bending analysis of functionally graded nanoplates based on a higher-order shear deformation theory using dynamic relaxation method. Tahouneh [15] studied free vibration analysis of bidirectional functionally graded annular plates resting on elastic foundations using differential quadrature method. Abdelrahman [16] developed effect of material transverse distribution profile on buckling of thick functionally graded material plates according to TSDT. Taj et al. [17] used finite element analysis of functionally graded sandwich plates under nonlinear sense for aerospace applications. Recently Yoosefian et al. [18] developed nonlinear bending of functionally graded sandwich plates under mechanical and thermal load. Thai et al. [19] studied bending of Symmetric Sandwich FGM Beams with Shear Connectors. Van Vinh et al. [20] developed an improved first-order mixed plate element for static bending and free vibration analysis of functionally graded sandwich plates. Sofiyev [21] developed the vibration and buckling of sandwich cylindrical shells covered by different coatings subjected to the hydrostatic pressure.

To the best of our knowledge, there has been no investigation on the bending of FGM sandwich plates using Finite Element Analysis (FEA) and at the same time comparing it with the four variable plate theory (RPT). This work aims to develop a simple higher order shear deformation theory (RPT) for the bending analyses of FG sandwich plates. The proposed theory has only four unknowns and four governing equations, but it satisfies the stress-free boundary conditions on the top and bottom surfaces of the sandwich plate without requiring any shear correction factors. Analytical solutions are obtained for sandwich plate with FG face sheets and its accuracy is verified by comparing the obtained results with those reported in the literature and the FEA implementation. The effects of several variables, such as thickness aspect ratios, gradient index and sandwich plate type on bending of FG sandwich plate are all investigated and discussed.

## 2. Problem Formulation

### 2.1. Preliminary concepts and definitions

The geometry and dimensions of the rectangular plate made of FGMs under consideration are represented in Fig. 1. Rectangular Cartesian coordinates $(x, y, z)$ are used to describe infinitesimal deformations of a three-layer sandwich elastic plate occupying the region $[0, a] \times [0, b] \times [-h/2, h/2]$ in the unstressed reference configuration, and the axes are parallel to the edges of the plate. The plate has length a, width b, and uniform thickness h. The mid-plane of the composite sandwich plate is defined by $z = 0$ and its external bounding planes being defined by $z = \pm h/2$. The vertical positions of the bottom surface, the two interfaces between the core and faces layers, and the top surface are denoted, respectively, $h_1 = -h/2$, $h_2$, $h_3$ and $h_4 = +h/2$.

The face layers of the sandwich plate are made of an isotropic material with material properties varying smoothly in the z (thickness) direction only. The core layer is made of an isotropic homogeneous material, as shown in Fig. 2. For brevity, the ratio of the thickness of each layer from bottom to top is denoted by the combination of three numbers, i.e., "1-0-1", "2-1-2" and so on. The volume fraction of the FGMs is assumed to obey a power-law function along the thickness direction as shown below:

$$V^{(1)}(z) = \left( \frac{z - h_2}{h_1 - h_2} \right)^k \tag{1a}$$

$$V^{(2)}(z) = 1 \tag{1b}$$

$$V^{(3)}(z) = \left( \frac{z - h_3}{h_4 - h_3} \right)^k \tag{1c}$$

where $h_1$, $h_2$ and $h_3$ are the bottom surface coordinates of the bottom face layer, the core layer and the top layer, respectively. Likewise, $h_2$, $h_3$ and $h_4$ are the top surface coordinates of the bottom face layer, the core layer and the top layer, respectively. In Eq. (1), $k$ indicates the power-law coefficient (volume fraction index). When $k = 0$, the material of plate becomes homogeneous ceramic.

The effective material properties, such as Young's modulus E, Poisson's ratio $\nu$, and thermal expansion coefficient $\alpha$ can be then expressed by the rule of mixture, as follows:

$$P^{(n)}(z) = (P_1 - P_2)V^{(n)} + P_2 \tag{2}$$

where $P^{(n)}$ is the effective material property of FGM of layer n. Note that $P_1$ and $P_2$ are the properties of the top and bottom faces of layer 1, respectively, and vice versa for layer 3 depending on the volume fraction $V^{(n)}$ (n = 1, 2, 3).
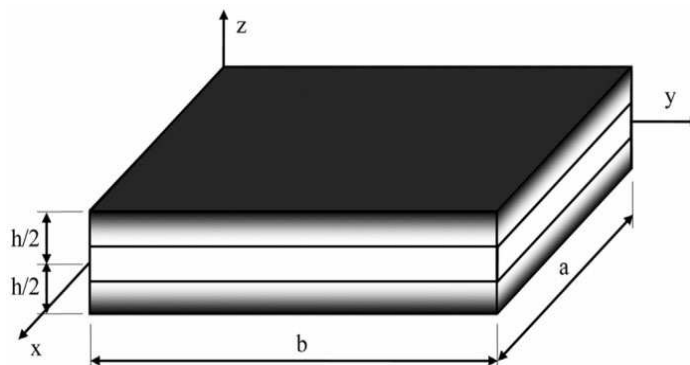


**Fig. 1.** Geometry of the functionally graded sandwich plate.
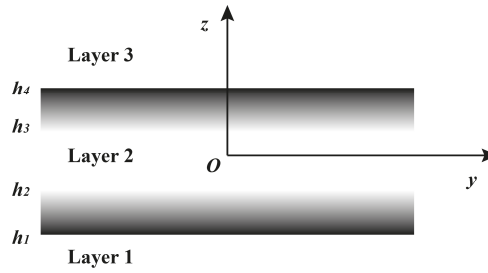
**Fig. 2.** The material variation along the thickness of the FGM sandwich plate.

## 2.2. Displacement field and strains

The in-plane displacement $u$, $v$ is assumed in $x$ and $y$ directions and transverse displacement $w$ in $z$ direction in the multi-directional FGM sandwich plate. In-plane and transverse displacements with consideration of the refined shear deformation theory can be written as [11]:

$$u(x,y,z) = u_0(x,y) - z\frac{\partial w_b}{\partial x} - f(z)\frac{\partial w_b}{\partial x}$$
$$v(x,y,z) = v_0(x,y) - z\frac{\partial w_b}{\partial y} - f(z)\frac{\partial w_b}{\partial y}$$ (3)
$$w(x,y,z) = w_b(x,y) + w_s(x,y)$$

where,

$$f(z) = -\frac{1}{4}z + \frac{5}{3}z\left(\frac{z}{h}\right)^2$$ (4)

in which $u_0$, $v_0$, $w_b$ and $w_s$ are in-plane and transverse displacements at the middle plane, respectively. The strains associated with the displacements in Eq. (3) are:

$$\varepsilon_x = \varepsilon_x^0 + z\,k_x^b + f(z)\,k_x^s$$
$$\varepsilon_y = \varepsilon_y^0 + z\,k_y^b + f(z)k_y^s$$
$$\gamma_{xy} = \gamma_{xy}^0 + z\,k_{xy}^b + f(z)\,k_{xy}^s$$
$$\gamma_{yz} = g(z)\,\gamma_{yz}^s$$ (5)
$$\gamma_{xz} = g(z)\,\gamma_{xz}^s$$
$$\varepsilon_z = 0$$

where,

$$\varepsilon_x^0 = \frac{\partial u_0}{\partial x}, \quad k_x^b = -\frac{\partial^2 w_b}{\partial x^2}, \quad k_x^s = -\frac{\partial^2 w_s}{\partial x^2}$$

$$\varepsilon_y^0 = \frac{\partial v_0}{\partial y}, \quad k_y^b = -\frac{\partial^2 w_b}{\partial y^2}, \quad k_y^s = -\frac{\partial^2 w_s}{\partial y^2}$$

$$\gamma_{xy}^0 = \frac{\partial u_0}{\partial y} + \frac{\partial v_0}{\partial x}, \quad k_{xy}^b = -2\frac{\partial^2 w_b}{\partial x\partial y}, \quad k_{xy}^s = -2\frac{\partial^2 w_s}{\partial x\partial y}$$ (6)

$$\gamma_{yz}^s = \frac{\partial w_s}{\partial y}, \quad \gamma_{xz}^s = \frac{\partial w_s}{\partial x}$$

$$g(z) = 1 - f'(z) = \frac{5}{4} - 5\left(\frac{z}{h}\right)^2$$

The stress-strain relationship for multi-directional FGM sandwich plate can be written as:

$$\begin{Bmatrix} \sigma_x \\ \sigma_y \\ \tau_{xy} \end{Bmatrix}^{(n)} = \begin{bmatrix} Q_{11} & Q_{12} & 0 \\ Q_{12} & Q_{22} & 0 \\ 0 & 0 & Q_{66} \end{bmatrix}^{(n)} \begin{Bmatrix} \varepsilon_x \\ \varepsilon_y \\ \gamma_{xy} \end{Bmatrix}$$ (7a)

and,

$$\begin{Bmatrix} \tau_{yz} \\ \tau_{zx} \end{Bmatrix}^{(n)} = \begin{bmatrix} Q_{44} & 0 \\ 0 & Q_{55} \end{bmatrix}^{(n)} \begin{Bmatrix} \gamma_{yz} \\ \gamma_{zx} \end{Bmatrix}$$ (7b)

where,

$$Q_{11}^{(n)}(z) = Q_{22}^{(n)}(z) = \frac{E^{(n)}(z)}{1-\nu^2}$$ (8a)

$$Q_{12}(z) = \nu Q_{11}^{(n)}(z) \tag{8b}$$

$$Q_{44}^{(n)}(z) = Q_{55}^{(n)} = Q_{66}^{(n)} = \frac{E^{(n)}(z)}{2(1+\nu)} \tag{8c}$$

### 2.3. Governing equations

The governing equations of equilibrium can be derived by using the principle of virtual displacements. The principle of virtual work in the present case yields:

$$\int_{-h/2}^{h/2} \int_A \left[ \sigma_x \delta\ \varepsilon_x + \sigma_y \delta\ \varepsilon_y + \tau_{xy} \delta\ \gamma_{xy} + \tau_{yz} \delta\ \gamma_{yz} + \tau_{xz} \delta\ \gamma_{xz} \right] dA\ dz - \int_A q(x,y)\delta\ w dA = 0 \tag{9}$$

where $A$ is the top surface and $q$ is the applied transverse load. Substituting Eqs. (5) and (7) into Eq. (9) and integrating through the thickness of the plate, Eq. (9) can be rewritten as:

$$\int_A \left[ N_x \delta\ \varepsilon_x^0 + N_y \delta\ \varepsilon_y^0 + N_{xy}\delta\ \varepsilon_{xy}^0 + M_x^b \delta\ k_x^b + M_y^b \delta\ k_y^b + M_{xy}^b \delta\ k_{xy}^b + M_x^s \delta\ k_x^s + M_y^s \delta\ k_y^s + M_{xy}^s \delta\ k_{xy}^s + S_{yz}^s \delta\ \gamma_{yz}^s + S_{xz}^s \delta\ \gamma_{xz}^s \right] dA - \int_A q(\delta\ w_b + \delta w_s) dA = 0 \tag{10}$$

where,

$$(N_x, N_y, N_{xy}) = \sum_{n=1}^{3} \int_{h_n}^{h_{n+1}} (\sigma_x, \sigma_y, \tau_{xy}) dz$$

$$(M_x^b, M_y^b, M_{xy}^b) = \sum_{n=1}^{3} \int_{h_n}^{h_{n+1}} (\sigma_x, \sigma_y, \tau_{xy}) z dz$$

$$(M_x^s, M_y^s, M_{xy}^s) = \sum_{n=1}^{3} \int_{h_n}^{h_{n+1}} (\sigma_x, \sigma_y, \tau_{xy}) f(z) dz \tag{11}$$

$$(S_{xz}^s, S_{yz}^s) = \sum_{n=1}^{3} \int_{h_n}^{h_{n+1}} (\tau_{xz}, \tau_{yz}) g(z) dz$$

Substituting Eq. (7) into Eq. (11) and integrating through the thickness of the plate, the stress resultants are given as:

$$\begin{Bmatrix} N \\ M^b \\ M^s \end{Bmatrix} = \begin{bmatrix} A & B & B^s \\ B & D & D^s \\ B^s & D^s & H^s \end{bmatrix} \begin{Bmatrix} \varepsilon \\ k^b \\ k^s \end{Bmatrix} \tag{12a}$$

$$\begin{Bmatrix} S_{yz}^s \\ S_{xz}^s \end{Bmatrix} = \begin{bmatrix} A_{44}^s & 0 \\ 0 & A_{55}^s \end{bmatrix} \begin{Bmatrix} \gamma_{yz}^s \\ \gamma_{xz}^s \end{Bmatrix} \tag{12b}$$

in which,

$$N = \left\{ N_x, N_y, N_{xy} \right\}^T, \quad M^b = \left\{ M_x^b, M_y^b, M_{xy}^b \right\}^T, \quad M^s = \left\{ M_x^s, M_y^s, M_{xy}^s \right\}^T, \tag{13a}$$

$$\varepsilon = \left\{ \varepsilon_x^0, \varepsilon_y^0, \gamma_{xy}^0 \right\}^T, \quad k^b = \left\{ k_x^b, k_y^b, k_{xy}^b \right\}^T, \quad k^s = \left\{ k_x^s, k_y^s, k_{xy}^s \right\}^T, \tag{13b}$$

$$A = \begin{bmatrix} A_{11} & A_{12} & 0 \\ A_{12} & A_{22} & 0 \\ 0 & 0 & A_{66} \end{bmatrix}, \quad B = \begin{bmatrix} B_{11} & B_{12} & 0 \\ B_{12} & B_{22} & 0 \\ 0 & 0 & B_{66} \end{bmatrix}, \quad D = \begin{bmatrix} D_{11} & D_{12} & 0 \\ D_{12} & D_{22} & 0 \\ 0 & 0 & D_{66} \end{bmatrix}, \tag{13c}$$

$$B^s = \begin{bmatrix} B_{11}^s & B_{12}^s & 0 \\ B_{12}^s & B_{22}^s & 0 \\ 0 & 0 & B_{66}^s \end{bmatrix}, \quad D^s = \begin{bmatrix} D_{11}^s & D_{12}^s & 0 \\ D_{12}^s & D_{22}^s & 0 \\ 0 & 0 & D_{66}^s \end{bmatrix}, \quad H^s = \begin{bmatrix} H_{11}^s & H_{12}^s & 0 \\ H_{12}^s & H_{22}^s & 0 \\ 0 & 0 & H_{66}^s \end{bmatrix}, \tag{13d}$$

$$S = \left\{ S_{xz}^s, S_{yz}^s \right\}^t, \quad \gamma = \left\{ \gamma_{xz}^0, \gamma_{yz}^0 \right\}^t, \quad A^s = \begin{bmatrix} A_{44}^s & 0 \\ 0 & A_{55}^s \end{bmatrix}, \tag{13e}$$

and the stiffness components are given as:

$$\begin{bmatrix} A_{11} & B_{11} & D_{11} & B_{11}^s & D_{11}^s & H_{11}^s \\ A_{12} & B_{12} & D_{12} & B_{12}^s & D_{12}^s & H_{12}^s \\ A_{66} & B_{66} & D_{66} & B_{66}^s & D_{66}^s & H_{66}^s \end{bmatrix} = \sum_{n=1}^{3} \int_{h_n}^{h_{n+1}} Q_{ij}^{(n)} (1, z, z^2, f(z), z\ f(z), f^2(z)) \begin{Bmatrix} 1 \\ \nu \\ \dfrac{1-\nu}{2} \end{Bmatrix} dz \tag{14a}$$

$$\left(A_{22},B_{22},D_{22},B_{22}^s,D_{22}^s,H_{22}^s\right)=\left(A_{11},B_{11},D_{11},B_{11}^s,D_{11}^s,H_{11}^s\right) \tag{14b}$$

$$A_{44}^s = A_{55}^s = \sum_{n=1}^{3}\int_{-h/2}^{h/2}Q_{ij}^{(n)}\left[g(z)\right]^2 dz \tag{14c}$$

The governing equations of equilibrium can be derived from Eq. (10) by integrating the displacement gradients by parts and setting the coefficients $\delta u_0$, $\delta v_0$, $\delta w_b$ and $\delta w_s$ to zero separately. Thus, one can obtain the equilibrium equations associated with the present shear deformation theory:

$$
\begin{aligned}
&\delta\ u_0\ :\quad \frac{\partial N_x}{\partial x}+\frac{\partial N_{xy}}{\partial y}=0 \\[4pt]
&\delta\ v_0\ :\quad \frac{\partial N_{xy}}{\partial x}+\frac{\partial N_y}{\partial y}=0 \\[4pt]
&\delta\ w_b\ :\quad \frac{\partial^2 M_x^b}{\partial x^2}+2\frac{\partial^2 M_{xy}^b}{\partial x\partial y}+\frac{\partial^2 M_y^b}{\partial y^2}+q=0 \\[4pt]
&\delta\ w_s\ :\quad \frac{\partial^2 M_x^s}{\partial x^2}+2\frac{\partial^2 M_{xy}^s}{\partial x\partial y}+\frac{\partial^2 M_y^s}{\partial y^2}+\frac{\partial S_{xz}^s}{\partial x}+\frac{\partial S_{yz}^s}{\partial y}+q=0
\end{aligned}
\tag{15}
$$

By introducing Eq. (12) into Eq. (15), the equations of motion can be expressed in terms of displacements $(u_0,\ v_0,\ w_b,\ w_s)$ and the appropriate equations take the form:

$$A_{11}\frac{\partial^2 u_0}{\partial x^2}+A_{66}\frac{\partial^2 u_0}{\partial y^2}+\left(A_{12}+A_{66}\right)\frac{\partial^2 v_0}{\partial x\partial y}-B_{11}\frac{\partial^3 w_b}{\partial x^3}-\left(B_{12}+2B_{66}\right)\frac{\partial^3 w_b}{\partial x\partial y^2}-B_{11}^s\frac{\partial^3 w_s}{\partial x^3}-\left(B_{12}^s+2B_{66}^s\right)\frac{\partial^3 w_s}{\partial x\partial y^2}=0, \tag{16a}$$

$$\left(A_{12}+A_{66}\right)\frac{\partial^2 u_0}{\partial x\partial y}+A_{66}\frac{\partial^2 v_0}{\partial x^2}+A_{22}\frac{\partial^2 v_0}{\partial y^2}-\left(B_{12}+2B_{66}\right)\frac{\partial^3 w_b}{\partial x^2\partial y}-B_{22}\frac{\partial^3 w_b}{\partial y^3}-B_{22}^s\frac{\partial^3 w_s}{\partial y^3}-\left(B_{12}^s+2B_{66}^s\right)\frac{\partial^3 w_s}{\partial x^2\partial y}=0, \tag{16b}$$

$$
\begin{aligned}
&B_{11}\frac{\partial^3 u_0}{\partial x^3}+\left(B_{12}+2B_{66}\right)\frac{\partial^3 u_0}{\partial x\partial y^2}+\left(B_{12}+2B_{66}\right)\frac{\partial^3 v_0}{\partial x^2\partial y}+B_{22}\frac{\partial^3 v_0}{\partial y^3}-D_{11}\frac{\partial^4 w_b}{\partial x^4}-2\left(D_{12}+2D_{66}\right)\frac{\partial^4 w_b}{\partial x^2\partial y^2} \\[4pt]
&-D_{22}\frac{\partial^4 w_b}{\partial y^4}-D_{11}^s\frac{\partial^4 w_s}{\partial x^4}-2\left(D_{12}^s+2D_{66}^s\right)\frac{\partial^4 w_s}{\partial x^2\partial y^2}-D_{22}^s\frac{\partial^4 w_s}{\partial y^4}+q=0,
\end{aligned}
\tag{16c}
$$

$$
\begin{aligned}
&B_{11}^s\frac{\partial^3 u_0}{\partial x^3}+\left(B_{12}^s+2B_{66}^s\right)\frac{\partial^3 u_0}{\partial x\partial y^2}+\left(B_{12}^s+2B_{66}^s\right)\frac{\partial^3 v_0}{\partial x^2\partial y}+B_{22}^s\frac{\partial^3 v_0}{\partial y^3}-D_{11}^s\frac{\partial^4 w_b}{\partial x^4}-2\left(D_{12}^s+2D_{66}^s\right)\frac{\partial^4 w_b}{\partial x^2\partial y^2} \\[4pt]
&-D_{22}^s\frac{\partial^4 w_b}{\partial y^4}-H_{11}^s\frac{\partial^4 w_s}{\partial x^4}-2\left(H_{12}^s+2H_{66}^s\right)\frac{\partial^4 w_s}{\partial x^2\partial y^2}-H_{22}^s\frac{\partial^4 w_s}{\partial y^4}+A_{55}^s\frac{\partial^2 w_s}{\partial x^2}+A_{44}^s\frac{\partial^2 w_s}{\partial y^2}+q=0.
\end{aligned}
\tag{16d}
$$

Clearly, when the effect of transverse shear deformation is neglected, Eq. (16) yields the equations of motion of FG plate based on the CPT.

## 2.4. Navier solution for simply supported rectangular FGM sandwich plate

The Navier solution method is employed to determine the analytical solutions for which the displacement variables are written as product of arbitrary parameters and known trigonometric functions to respect the equations of motion and boundary conditions:

$$
\begin{Bmatrix} u_0 \\ v_0 \\ w_b \\ w_s \end{Bmatrix}=\sum_{m=1}^{\infty}\sum_{n=1}^{\infty}\begin{Bmatrix} U_{mn}\cos(\lambda\ x)\sin(\mu\ y) \\ V_{mn}\sin(\lambda\ x)\cos(\mu\ y) \\ W_{bmn}\sin(\lambda\ x)\sin(\mu\ y) \\ W_{smn}\sin(\lambda\ x)\sin(\mu\ y) \end{Bmatrix}
\tag{17}
$$

where $U_{mn}$, $V_{mn}$, $W_{bmn}$ and $W_{smn}$ are arbitrary parameters to be determined, $\lambda = m\pi/a$ and $\mu = n\pi/b$. The transverse load $q$ is also expanded in the double-Fourier series as:

$$q(x,y)=\sum_{m=1}^{\infty}\sum_{n=1}^{\infty}q_{mn}\sin\left(\lambda x\right)\sin\left(\mu y\right) \tag{18}$$

For the case of a sinusoidally distributed load, we have:

$$m = n = 1 \ \text{ and } \ q_{11}=q_0 \tag{19}$$

and in the case of uniformly distributed load, we have:

$$q_{mn}=\begin{cases} \dfrac{12q_0}{mn\pi^2}, & \text{For odd } m,n \\[6pt] 0, & \text{For even } m,n \end{cases} \tag{20}$$

where $q_0$ represents the intensity of the load at the plate center.

Substituting Eq. (17) and (18) into Eq. (16), the following problem is obtained:

$$\begin{bmatrix} a_{11} & a_{12} & a_{13} & a_{14} \\ a_{12} & a_{22} & a_{23} & a_{24} \\ a_{13} & a_{23} & a_{33} & a_{34} \\ a_{14} & a_{24} & a_{34} & a_{44} \end{bmatrix} \begin{Bmatrix} U_{mn} \\ V_{mn} \\ W_{bmn} \\ W_{smn} \end{Bmatrix} = \begin{Bmatrix} 0 \\ 0 \\ q_{mn} \\ q_{mn} \end{Bmatrix} \tag{21}$$

where,

$$\begin{cases} a_{11} = A_{11}\lambda^2 + A_{66}\mu^2, \\ a_{12} = \lambda\mu\left(A_{12} + A_{66}\right) \\ a_{13} = -\lambda\left(B_{11}\lambda^2 + \left(B_{12} + 2B_{66}\right)\mu^2\right), \\ a_{14} = -\lambda\left(B_{11}^s\lambda^2 + \left(B_{12}^s + 2B_{66}^s\right)\mu^2\right), \\ a_{22} = A_{66}\lambda^2 + A_{22}\mu^2, \\ a_{23} = -\mu\left(\left(B_{12} + 2B_{66}\right)\lambda^2 + B_{22}\mu^2\right), \\ a_{24} = -\mu\left(\left(B_{12}^s + 2B_{66}^s\right)\lambda^2 + B_{22}^s\mu^2\right), \\ a_{33} = D_{11}\lambda^4 + 2(D_{12} + 2D_{66})\lambda^2\mu^2 + D_{22}\mu^4, \\ a_{34} = D_{11}^s\lambda^4 + 2\left(D_{12}^s + 2D_{66}^s\right)\lambda^2\mu^2 + D_{22}^s\mu^4, \\ a_{44} = D_{11}^s\lambda^4 + 2\left(D_{12}^s + 2D_{66}^s\right)\lambda^2\mu^2 + D_{22}^s\mu^4, \end{cases} \tag{22}$$

## 3. Numerical Results and Discussions

Functionally graded sandwich plate based on the present higher order shear deformation model is considered here. Some representative results of the Navier solution obtained for a simply supported rectangular sandwich plate are presented in detail.

Unless mentioned otherwise, a simply supported Al/Al$_2$O$_3$ sandwich plate composed of Aluminum face sheets (as metal) and an Alumina core (as ceramic) is studied. The following material properties have been used:

Metal (Aluminium, Al): $E_m = 70$ GPa; Poisson's ratio $\nu = 0.3$.

Ceramic (Alumina, Al$_2$O$_3$): $E_c = 151$ GPa; Poisson's ratio $\nu = 0.3$.

Several kinds of sandwich plates are presented according to the thickness of the core layer which is fully ceramic while the bottom and top surface of the plate are metal-rich.

- The (1-0-1) FGM sandwich plate: The plate is symmetric and made of only two equal-thickness FGM layers, that is, there is no core layer. Thus, $h_1 = h_2 = 0$.
- The (1-1-1) FGM sandwich plate: The plate is symmetric and made of three equal thickness layers. In this case, we have, $h_1 = -h/6$, $h_2 = h/6$.
- The (2-1-2) FGM sandwich plate: The plate is symmetric and we have: $h_1 = -h/10$, $h_2 = h/10$.
- The (2-2-1) FGM sandwich plate: The plate is non-symmetric and we have: $h_1 = -h/10$, $h_2 = 3h/10$.
- The (1-2-1) FGM sandwich plate: The plate is symmetric and we have $h_1 = -h/4$, $h_2 = h/4$.

For convenience, and mathematical clarity, the following dimensionless of the equations are used:

Central deflection $\overline{W}$:

$$\overline{W} = \frac{10hE_0}{q_0 a^2} w\left(\frac{a}{2}, \frac{b}{2}\right) \tag{23}$$

Axial stress $\overline{\sigma}_x$:

$$\overline{\sigma}_x = \frac{10.h^2}{q_0 a^2} \sigma_x\left(\frac{a}{2}, \frac{b}{2}, z\right) \tag{24}$$

Shear stress $\overline{\tau}_{xz}$:

$$\overline{\tau}_{xz} = \frac{h}{q_0 a} \tau_{xz}\left(0, \frac{b}{2}, z\right) \tag{25}$$

where $E_0 = 1$ GPa. It has to be noted that the deflections are calculated at the $X = a/2$, $Y = b/2$, the distribution of axial stress is presented at the cross-section $X = a/2$, $Y = b/2$ in though $Z$ direction and the distribution of shear stress is presented at the cross-section $X = 0$, $Y = b/2$ in though $Z$ direction.

In order to prove the validity of the presented higher-order shear deformation plate theory, some comparisons are made between the results obtained from this theory and those obtained by Zenkour [22] based on sinusoidal shear deformation theory (SSDPT), trigonometric shear deformation theory (TSDPT), the first-order shear deformation theory (FSDPT), the simple higher order shear deformation theory developed by Meksi et al. [23] and the present results of FEA as given in Tables 1 to 3.

From these tables, there is a good agreement between the results of the present theory with other theories and the FEA except for the case of transverse shear stress $\overline{\tau}_{xz}$. A small difference between the results is seen (see Table 3). This is due to the different approaches used to predict the transverse shear stresses. It is clear that the FSDPT violates the stress-free boundary conditions on the plate surface, and consequently, a shear correction factor is required. Finally, it is important to note that the present theory involves only four unknowns vs five in the case of SSDPT, TSDPT and FSDPT. Besides, it does not require a shear correction factor as in the case of FSDPT.

**Table 1.** Comparisons of dimensionless deflection $\overline{W}$ of simply supported square power-law FGM plates with other theories ($a/h$ = 10).

| k | Theory | $\overline{W}$ | | | | |
|---|---|---|---|---|---|---|
| | | 1-0-1 | 2-1-2 | 1-1-1 | 2-2-1 | 1-2-1 |
| 0 | Present (FEA) | 0.2131 | 0.2131 | 0.2131 | 0.2131 | 0.2131 |
| | Present (Analytical solution) | 0.1961 | 0.1961 | 0.1961 | 0.1961 | 0.1961 |
| | Meksi et al. [23] | 0.1958 | 0.1958 | 0.1958 | 0.1958 | 0.1958 |
| | SSDPT [22] | 0.1960 | 0.1960 | 0.1960 | 0.1960 | 0.1960 |
| | TSDPT [22] | 0.1960 | 0.1960 | 0.1960 | 0.1960 | 0.1960 |
| | FSDPT [22] | 0.1961 | 0.1961 | 0.1961 | 0.1961 | 0.1961 |
| | CPT [22] | 0.1856 | 0.1856 | 0.1856 | 0.1856 | 0.1856 |
| 1 | Present (FEA) | 0.3468 | 0.3280 | 0.3126 | 0.3012 | 0.2905 |
| | Present (Analytical solution) | 0.3236 | 0.3063 | 0.2919 | 0.2808 | 0.2709 |
| | Meksi et al. [23] | 0.3236 | 0.3063 | 0.2919 | 0.2801 | 0.2707 |
| | SSDPT [22] | 0.3235 | 0.3062 | 0.2919 | 0.2808 | 0.2709 |
| | TSDPT [22] | 0.3235 | 0.3063 | 0.2919 | 0.2808 | 0.2709 |
| | FSDPT [22] | 0.3248 | 0.3075 | 0.2930 | 0.2816 | 0.2716 |
| | CPT [22] | 0.3105 | 0.2941 | 0.2802 | 0.2692 | 0.2595 |
| 2 | Present (FEA) | 0.4002 | 0.3765 | 0.3554 | 0.3382 | 0.3233 |
| | Present (Analytical solution) | 0.3733 | 0.3523 | 0.3328 | 0.3161 | 0.3026 |
| | Meksi et al. [23] | 0.3736 | 0.3525 | 0.3330 | 0.3161 | 0.3025 |
| | SSDPT [22] | 0.3731 | 0.3521 | 0.3328 | 0.3161 | 0.3026 |
| | TSDPT [22] | 0.3733 | 0.3523 | 0.3329 | 0.3162 | 0.3026 |
| | FSDPT [22] | 0.3751 | 0.3540 | 0.3344 | 0.3173 | 0.3037 |
| | CPT [22] | 0.3588 | 0.3394 | 0.3206 | 0.3040 | 0.2909 |
| 5 | Present (FEA) | 0.4408 | 0.4196 | 0.3963 | 0.3744 | 0.3567 |
| | Present (Analytical solution) | 0.4092 | 0.3918 | 0.3714 | 0.3496 | 0.3348 |
| | Meksi et al. [23] | 0.4097 | 0.3924 | 0.3718 | 0.3497 | 0.3348 |
| | SSDPT [22] | 0.4090 | 0.3916 | 0.3712 | 0.3495 | 0.3347 |
| | TSDPT [22] | 0.4092 | 0.3918 | 0.3714 | 0.3496 | 0.3348 |
| | FSDPT [22] | 0.4112 | 0.3941 | 0.3735 | 0.3512 | 0.3363 |
| | CPT [22] | 0.3922 | 0.3778 | 0.3586 | 0.3369 | 0.3228 |
| 10 | Present (FEA) | 0.4514 | 0.4337 | 0.4116 | 0.3892 | 0.3705 |
| | Present (Analytical solution) | 0.4177 | 0.4040 | 0.3855 | 0.3621 | 0.3482 |
| | Meksi et al. [23] | 0.4179 | 0.4048 | 0.3861 | 0.3623 | 0.3484 |
| | SSDPT [22] | 0.4175 | 0.4037 | 0.3849 | 0.3491 | 0.3411 |
| | TSDPT [22] | 0.4177 | 0.4040 | 0.3855 | 0.3621 | 0.3482 |
| | FSDPT [22] | 0.4191 | 0.4065 | 0.3878 | 0.3639 | 0.3499 |
| | CPT [22] | 0.3987 | 0.3894 | 0.3723 | 0.3491 | 0.3361 |

**Table 2.** Comparisons of dimensionless axial stress $\overline{\sigma}_x$ of simply supported square power-law FGM plates with other theories ($a/h$ = 10).

| k | Theory | $\overline{\sigma}_x$ | | | | |
|---|---|---|---|---|---|---|
| | | 1-0-1 | 2-1-2 | 1-1-1 | 2-2-1 | 1-2-1 |
| 0 | Present (FEA) | 1.9580 | 1.9580 | 1.9580 | 1.9580 | 1.9580 |
| | Present (Analytical solution) | 1.9943 | 1.9943 | 1.9943 | 1.9943 | 1.9943 |
| | Meksi et al. [23] | 1.9882 | 1.9882 | 1.9882 | 1.9882 | 1.9882 |
| | SSDPT [22] | 2.0545 | 2.0545 | 2.0545 | 2.0545 | 2.0545 |
| | TSDPT [22] | 2.0498 | 2.0498 | 2.0498 | 2.0498 | 2.0498 |
| | FSDPT [22] | 1.9757 | 1.9757 | 1.9757 | 1.9757 | 1.9757 |
| 1 | Present (FEA) | 1.5970 | 1.5730 | 1.5580 | 1.5230 | 1.5820 |
| | Present (Analytical solution) | 1.5441 | 1.4627 | 1.3938 | 1.2882 | 1.2915 |
| | Meksi et al. [23] | 1.5404 | 1.4591 | 1.3902 | 1.2847 | 1.2879 |
| | SSDPT [22] | 1.5820 | 1.4985 | 1.4289 | 1.3234 | 1.3259 |
| | TSDPT [22] | 1.5792 | 1.4958 | 1.4261 | 1.3206 | 1.3230 |
| | FSDPT [22] | 1.5324 | 1.4516 | 1.3830 | 1.2774 | 1.2809 |
| 2 | Present (FEA) | 1.7220 | 1.6200 | 1.6020 | 1.5780 | 1.6000 |
| | Present (Analytical solution) | 1.7835 | 1.6865 | 1.5937 | 1.4367 | 1.4468 |
| | Meksi et al. [23] | 1.7796 | 1.6829 | 1.5900 | 1.4329 | 1.4431 |
| | SSDPT [22] | 1.8245 | 1.7241 | 1.6302 | 1.4738 | 1.4828 |
| | TSDPT [22] | 1.8216 | 1.7214 | 1.6274 | 1.4709 | 1.4798 |
| | FSDPT [22] | 1.7708 | 1.6749 | 1.5824 | 1.4252 | 1.4358 |
| 5 | Present (FEA) | 1.8990 | 1.8180 | 1.7210 | 1.7200 | 1.7210 |
| | Present (Analytical solution) | 1.9500 | 1.8768 | 1.7813 | 1.5759 | 1.6043 |
| | Meksi et al. [23] | 1.9458 | 1.8733 | 1.7778 | 1.5720 | 1.6006 |
| | SSDPT [22] | 1.9956 | 1.9154 | 1.8183 | 1.6147 | 1.6410 |
| | TSDPT [22] | 1.9927 | 1.9130 | 1.8158 | 1.6118 | 1.6381 |
| | FSDPT [22] | 1.9357 | 1.8647 | 1.7698 | 1.5640 | 1.5930 |
| 10 | Present (FEA) | 1.9370 | 1.8760 | 1.7860 | 1.7890 | 1.6830 |
| | Present (Analytical solution) | 1.9834 | 1.9340 | 1.8491 | 1.6281 | 1.6699 |
| | Meksi et al. [23] | 1.9787 | 1.9305 | 1.8457 | 1.6242 | 1.6663 |
| | SSDPT [22] | 2.0336 | 1.9731 | 1.8814 | 1.6197 | 1.6485 |
| | TSDPT [22] | 2.0303 | 1.9712 | 1.8837 | 1.6660 | 1.7041 |
| | FSDPT [22] | 1.9678 | 1.9216 | 1.8375 | 1.6164 | 1.6584 |

**Table 3.** Comparisons of dimensionless transverse shear stress $\bar{\tau}_{xz}$ of simply supported square power-law FGM plates with other theories ($a/h = 10$).

| $k$ | Theory | $\bar{\tau}_{xz}$ | | | | |
|---|---|---|---|---|---|---|
| | | 1-0-1 | 2-1-2 | 1-1-1 | 2-2-1 | 1-2-1 |
| 0 | Present (Analytical solution) | 0.2385 | 0.2385 | 0.2385 | 0.2385 | 0.2385 |
| | Meksi et al. [23] | 0.2027 | 0.2027 | 0.2027 | 0.2027 | 0.2027 |
| | SSDPT [22] | 0.2461 | 0.2461 | 0.2461 | 0.2461 | 0.2461 |
| | TSDPT [22] | 0.2385 | 0.2385 | 0.2385 | 0.2385 | 0.2385 |
| | FSDPT [22] | 0.1909 | 0.1909 | 0.1909 | 0.1909 | 0.1909 |
| 1 | Present (Analytical solution) | 0.2920 | 0.2710 | 0.2611 | 0.2595 | 0.2525 |
| | Meksi et al. [23] | 0.2577 | 0.2389 | 0.2287 | 0.2254 | 0.2184 |
| | SSDPT [22] | 0.2990 | 0.2777 | 0.2680 | 0.2668 | 0.2600 |
| | TSDPT [22] | 0.2920 | 0.2710 | 0.2611 | 0.2595 | 0.2525 |
| | FSDPT [22] | 0.2609 | 0.2431 | 0.2325 | 0.2276 | 0.2205 |
| 2 | Present (Analytical solution) | 0.3262 | 0.2883 | 0.2718 | 0.2693 | 0.2583 |
| | Meksi et al. [23] | 0.2924 | 0.2593 | 0.2424 | 0.2370 | 0.2260 |
| | SSDPT [22] | 0.3328 | 0.2942 | 0.2780 | 0.2762 | 0.2654 |
| | TSDPT [22] | 0.3262 | 0.2883 | 0.2718 | 0.2693 | 0.2583 |
| | FSDPT [22] | 0.2973 | 0.2675 | 0.2507 | 0.2431 | 0.2325 |
| 5 | Present (Analytical solution) | 0.3863 | 0.3145 | 0.2864 | 0.2826 | 0.2651 |
| | Meksi et al. [23] | 0.3465 | 0.2882 | 0.2609 | 0.2523 | 0.2358 |
| | SSDPT [22] | 0.3937 | 0.3193 | 0.2915 | 0.2889 | 0.2715 |
| | TSDPT [22] | 0.3863 | 0.3145 | 0.2864 | 0.2826 | 0.2651 |
| | FSDPT [22] | 0.3453 | 0.2973 | 0.2720 | 0.2609 | 0.2459 |
| 10 | Present (Analytical solution) | 0.4320 | 0.3324 | 0.2956 | 0.2908 | 0.2689 |
| | Meksi et al. [23] | 0.3818 | 0.3057 | 0.2717 | 0.2609 | 0.2413 |
| | SSDPT [22] | 0.4414 | 0.3364 | 0.2952 | 0.2967 | 0.2767 |
| | TSDPT [22] | 0.4320 | 0.3324 | 0.2956 | 0.2908 | 0.2689 |
| | FSDPT [22] | 0.3727 | 0.3131 | 0.2829 | 0.2699 | 0.2525 |

In Fig. 3, it is observed that, among the various power law indices, the variation of the volume fraction (and consequently of the modulus of elasticity) is highest at the internal points of the top and bottom Aluminum face sheets, while the material properties of the core remain unaffected by definition (see Eq. (1b)). In Fig. 4, the normal stress distributions across the dimensionless cross section thickness of the plate, normalized according to Eq. (24) are plotted. Two cases of cross section arrangement of the FGM plate are considered: (a) the 1-0-1 section and (b) the 1-2-1 section. It is observed that in the case of $k = 0$ (homogeneous ceramic material), the stress distribution is a nearly straight line, as expected for both cases of layer arrangement. At the top and bottom regions of the cross section, while the values of the stress distribution for the case $k = 1$ are lower than those in the homogeneous case, it is obvious that the stress distribution increases at these regions for increasing $k$. This happens because of the different properties of the Aluminum face sheets (as metal) and the Alumina core (as ceramic) and is justified by the configurations of the corresponding volume fraction distributions, as shown in Figs. 3(a) and 3(b), respectively. It is apparent in Fig. 4(a) that in the case of $k = 1$, the stress at the extreme upper and lower layers becomes minimum. Things get more complicated in Fig. 4(b), where the ceramic Alumina core layer is present, yielding indeed linear stress distributions ranging from -0.25 to 0.25 of the plate thickness, i.e., the middle half of the plate thickness, in accordance with the pattern 1-2-1. In this latter case, while the stress distribution for $k = 1$ appears to be concave near the top and bottom ends of the plate cross section, the stress distributions for $k = 2$ or larger show a different trend, which, beginning from the middle of the plate cross section, increases until a maximum value at the interface between the core and face layers, then decreases until a minimum value at a point inside the face layers. After this point it can increase or decrease until the plate extreme surface.
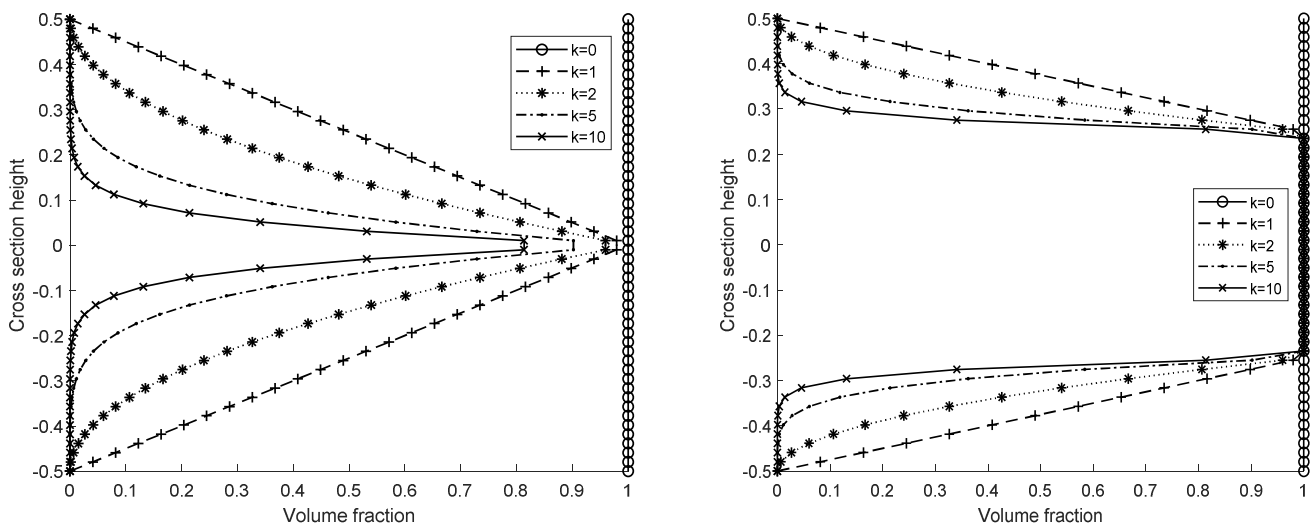


**Fig. 3.** Distributions of volume fraction ratio across the thickness of a FGM plate, for various values of power-law coefficient (volume fraction index).

(1-0-1) FGM sandwich plate

(1-2-1) FGM sandwich plate
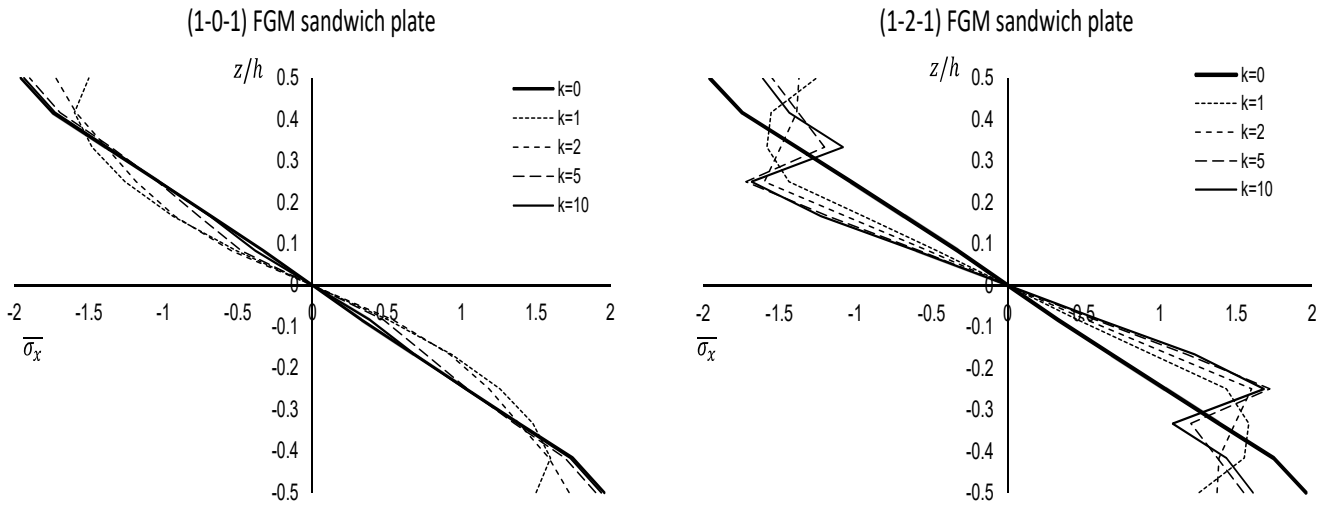


**Fig. 4.** Distributions of normalized normal stress across the thickness of simply supported square FGM plate, for various values of power-law coefficient (volume fraction index).

(1-0-1) FGM sandwich plate

(1-2-1) FGM sandwich plate
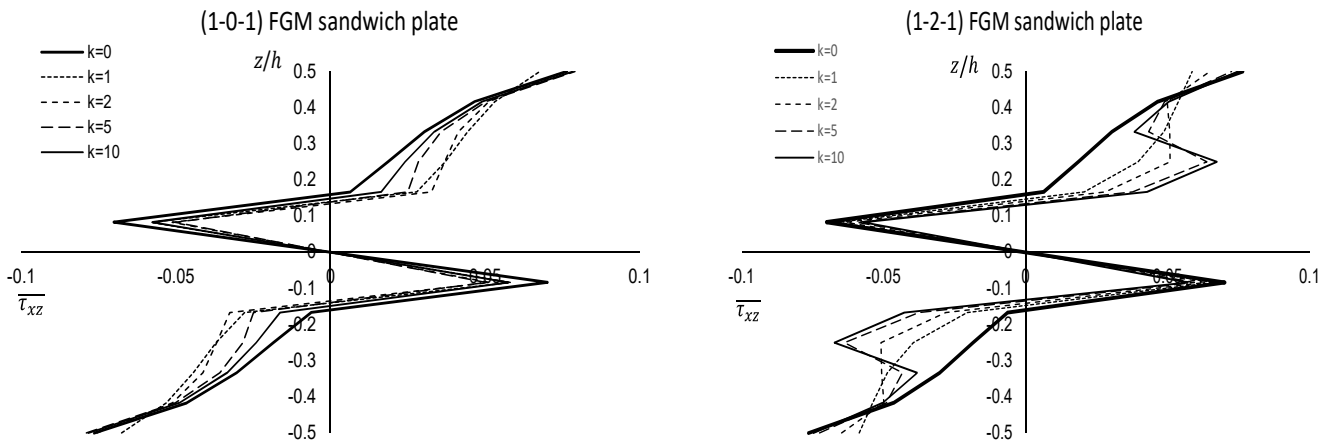


**Fig. 5.** Distributions of normalized shear stress across the thickness of simply supported square FGM plate, for various values of power-law coefficient (volume fraction index).

Except for different general configuration, similar trends to those described in the previous paragraph hold for the normalized shear stresses, as shown in Figs. 5(a) and 5(b) for the two-layer patterns 1-0-1 and 1-2-1, respectively. In this figure, the normalized shear stresses, according to Eq. (25), are plotted vs the dimensionless plate thickness height. In Fig. 4(a), the stress distributions for the cases $k = 0$ and $k = 10$ nearly coincide, as expected due to the volume fraction distributions shown in Fig. 3(a). In addition, the minimum and maximum trends observed for the normal stresses in Fig. 4(b) appear also in the shear stress distributions of Fig. 5(b).

A general observation for all stress distributions (both normal and shear) and for both layer patterns (1-0-1 and 1-2-1) shown in Figs. 4 and 5 is the fact that the maximum stress value occurs for the case of $k = 0$ and the minimum stress value at the extreme ends of the plate cross section occurs for $k = 1$, for all the cases considered.

In Fig. 6 the normal stresses, shear stresses and out of plane displacements are shown for the case of a simply supported plate with layer pattern 1-2-1 and power law exponent $k = 10$. Only half of the plate model is shown, in order to view the distributions across the thickness of the plate, for better understanding the stress and displacement fields. It is noted that the stress and displacement values are not normalized and reflect an actual case of FGM square plate model, with dimension 10 m, thickness 1 m. The intensity of the distributed load at the center of the plate is equal to 10.000 N/m². Normalizing the maximum values that appear in the contours according to Eqs. (23), (24) and (25), results in the normalized values that can be found in Tables 1, 2 and 3 of the present study for 1-2-1 and $k = 10$. The thickness of the plate is discretized into 12 C3D8 elements, while the side of the plate is discretized into 60 C3D8 elements. All modeling has been done in Abaqus software. It is observed that the deformed geometry of the plate is in accordance with its static loading and boundary conditions, whereas the normal stress distribution in Fig. 6(a) follows the trend of the corresponding plot in Fig. 4(b), in both in plane directions, due to the symmetry of the geometry, loading and boundary conditions of the plate.

(a)



(b)



(c)
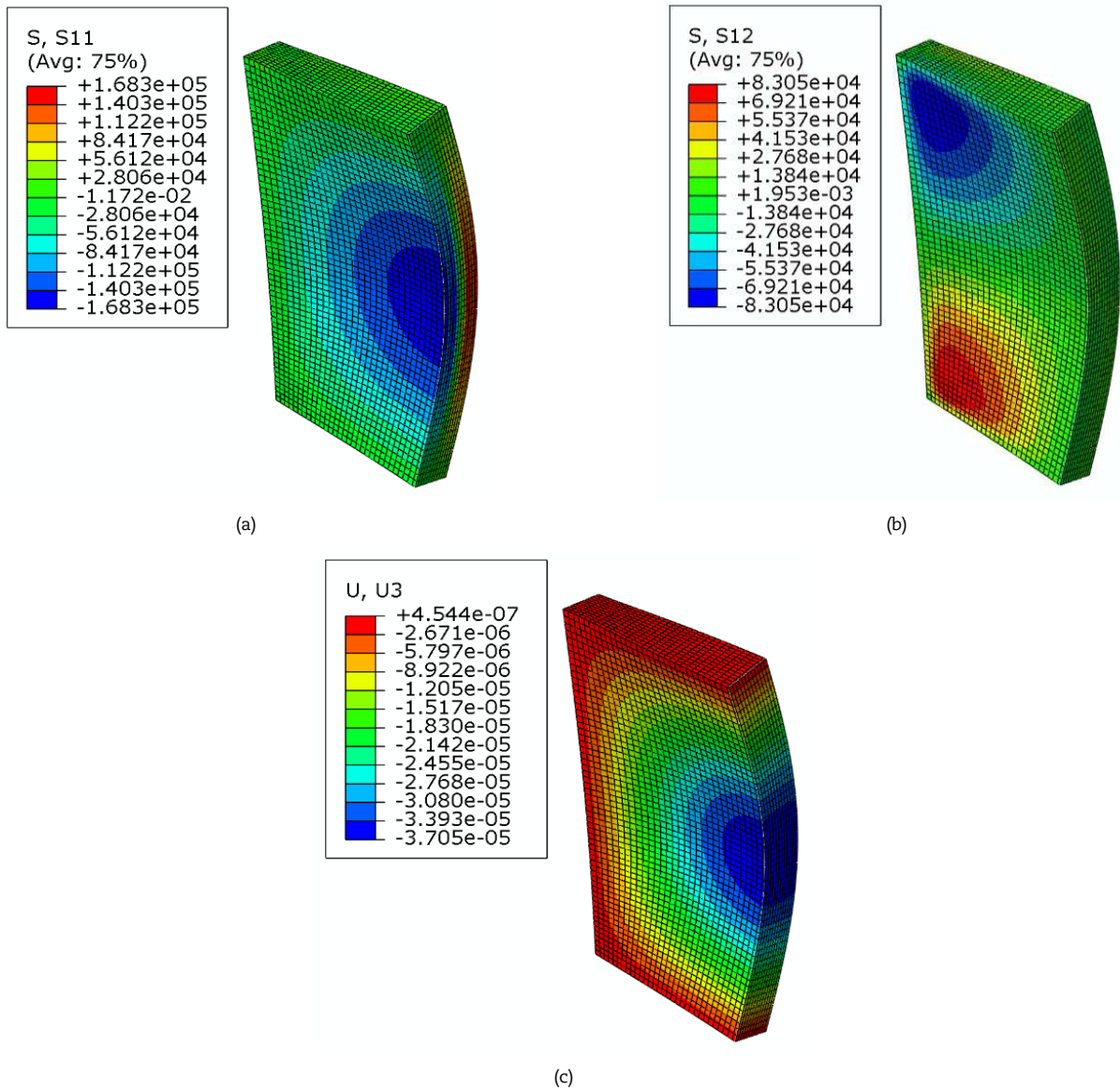
**Fig. 6.** Contours of the normal stress, shear stress and out of plane displacement of the simply supported FGM plate for layer pattern 1-2-1 and power law exponent $k = 10$.

## 4. Conclusion

A four-variable RPT and FEA were developed for the bending analysis of rectangular FG sandwich plate. The theory took into account the transverse shear effects and parabolic distribution of the transverse shear strains through the thickness of the FG sandwich plate. Hence, it was unnecessary to use shear correction factors. The power-law FGM sandwich plates with the FGM facesheet and the homogeneous core was considered.

Briefly, the following results were obtained:
- A good agreement between the results of the present theory with other theories and the FEA except for the case of transverse shear stress.
- The FSDPT violated the stress-free boundary conditions on the plate surface, and consequently, a shear correction factor was required.
- A general observation for all stress distributions (both normal and shear) and for both layer patterns (1-0-1 and 1-2-1) shown in figures is the fact that the maximum stress value occurs for the case of $k = 0$ and the minimum stress value at the extreme ends of the plate cross section occurs for $k = 1$, for all the cases considered.
- All comparison studies demonstrated that the present solution and FEA are highly efficient for the exact analysis of the bending of FG rectangular sandwich plates.
- The FEA is a valuable tool for analyzing the static bending response of FGM sandwich plates. It allows engineers and researchers to study complex material distributions and loading conditions, providing insights into the structural behavior and helping in the design and optimization of FGM composite structures.

In conclusion, it can be said that the proposed RPT theory is accurate, elegant and simple in solving the bending behavior of FG sandwich plates. However, it has to be noted that an improvement of the present theory may be necessary, especially when it is applied to a laminated structure to satisfy interlayer transverse shear stress continuity. The extension of the present theory is also envisaged for handling general boundary conditions.

## Author Contributions

L. Hadji planned the scheme, initiated the project, and developed the mathematical modeling. V. Plevris and G. Papazafeiropoulos examined the theory validation and analyzed the results. The manuscript was written through the contribution of all authors. All authors discussed the results, reviewed, and approved the final version of the manuscript.

## Acknowledgments

## Conflict of Interest

The authors declared no potential conflicts of interest with respect to the research, authorship, and publication of this article.

## Funding

## Data Availability Statements

The datasets generated and/or analyzed during the current study are available from the corresponding author on reasonable request.

## References

[1] Hohe, J., Librescu, L., Advances in the Structural Modeling of Elastic Sandwich Panels, *Mechanics of Advanced Materials and Structures*, 11, 2004, 395–424.
[2] Madan, R., Bhowmick, S., A review on application of FGM fabricated using solid-state processes, *Advances in Materials and Processing Technologies*, 6, 2020, 608–619.
[3] Suresh, S., Mortensen, A., Functionally graded metals and metal-ceramic composites: Part 2 Thermomechanical behavior, *International Materials Reviews*, 42(3), 1997, 85-116.
[4] Javaheri, R., Eslami, M.R., Buckling of functionally graded plates under in-plane compressive loading, *ZAMM Zeitschrift fur Angewandte Mathematik und Mechanik*, 82, 2002, 277–283.
[5] Reissner, E., The effect of transverse shear deformation on the bending of elastic plates, *Journal of Applied Mechanics*, 12(2), 1945, 69–77.
[6] Mindlin, R.D., Influence of rotary inertia and shear on flexural motions of isotropic elastic plates, *Journal of Applied Mechanics*, 18, 1951, 31–38.
[7] Reddy, J.N., A simple higher order shear deformation theory for laminated composite plates, *Journal of Applied Mechanics*, 51, 1984, 754–752.
[8] Tran, L.V., Ferreira, A.J.M., Xuan, H.N., Isogeometric analysis of functionally graded plates using higher-order shear deformation theory, *Composites: Part B*, 51, 2013, 368–383.
[9] Taj, G., Chakrabarti, A., Sheikh, A.H., Analysis of functionally graded plates using higher order shear deformation theory, *Applied Mathematical Modelling*, 37, 2013, 8484–8494.
[10] Oktem, A.S., Mantari, J.L., Soares, C.G., Static response of functionally graded plates and doubly-curved shells based on a higher order shear deformation theory, *European Journal of Mechanics - A/Solids*, 36, 2012, 163–172.
[11] Houari, M.S.A., Benyoucef, S., Mechab, I., Tounsi, A., Two variable refined plate theory for thermo elastic bending analysis of functionally graded sandwich plates, *Journal of Thermal Stresses*, 34, 2011, 315–334.
[12] Shaat, M., Alshorbagy, A.E., Alieldin, S.S., Meletis, E.I., Size-dependent analysis of functionally graded ultra-thin films, *Structural Engineering and Mechanics*, 44(4), 2012, 431-448.
[13] Malikan, M., Eremeyev, V.A., A new hyperbolic-polynomial higher-order elasticity theory for mechanics of thick FGM beams with imperfection in the material composition, *Composite Structures*, 249, 2020, 112486.
[14] Golmakani, M.E., Malikan, M., Pour, S.G., Eremeyev, V.A., Bending analysis of functionally graded nanoplates based on a higher-order shear deformation theory using dynamic relaxation method, *Continuum Mechanics and Thermodynamics*, 35, 2023, 1103–1122.
[15] Tahouneh, V., Free vibration analysis of bidirectional functionally graded annular plates resting on elastic foundations using differential quadrature method, *Structural Engineering and Mechanics*, 52(4), 2014, 663-686.
[16] Abdelrahman, W.G., Effect of material transverse distribution profile on buckling of thick functionally graded material plates according to TSDT, *Structural Engineering and Mechanics*, 71(1), 2020, 83-90.
[17] Taj, G., Chakrabarti, A., Malathy, R., Senthil Kumar, S.R.R., Finite element analysis of functionally graded sandwich plates under nonlinear sense for aerospace applications, *Structural Engineering and Mechanics*, 80(3), 2021, 341-353.
[18] Yoosefian, A.R., Golmakani, M.E., Sadeghian, M., Nonlinear bending of functionally graded sandwich plates under mechanical and thermal load, *Communications in Nonlinear Science and Numerical Simulation*, 84, 2020, 105161.
[19] Thai, D.N., Minh, P.V., Hoang, C.P., Duc, T.T., Thi Cam, N.N., Thi, D.N., Bending of Symmetric Sandwich FGM Beams with Shear Connectors, *Mathematical Problems in Engineering*, 2021, 2021, 7596300.
[20] Van Vinh, P., Belarbi, MO., Avcar, M., Civalek, O., An improved first-order mixed plate element for static bending and free vibration analysis of functionally graded sandwich plates, *Archive of Applied Mechanics*, 93, 2023, 1841–1862.
[21] Sofiyev, A.H., The vibration and buckling of sandwich cylindrical shells covered by different coatings subjected to the hydrostatic pressure, *Composite Structures*, 117, 2014, 124-134.
[22] Zenkour, A.M., A comprehensive analysis of functionally graded sandwich plates, Part1- deflection and stresses, *International Journal of Solids and Structures*, 42, 2005, 5224–5242.
[23] Meksi, R., Benyoucef, S., Mahmoudi, A., Tounsi, A., Adda Bedia, E.A., Mahmoud, S.R., An analytical solution for bending, buckling and vibration responses of FGM sandwich plates, *Journal of Sandwich Structures and Materials*, 21(2), 2019, 727-757.

## ORCID iD

Lazreg Hadji  https://orcid.org/0000-0002-3333-5902
Vagelis Plevris  https://orcid.org/ 0000-0002-7377-781X
George Papazafeiropoulos  https://orcid.org/ 0000-0002-9404-4447